International Journal of Fluid Power 12 (2011) No. 3 pp. 17-30

INVESTIGATION OF NOISE SOURCES ON A SERIES HYBRID TRANSMISSION

Richard Klop and Monika Ivantysynova

Purdue University, Department of Agricultural and Biological Engineering, 225 S. University St., West Lafayette, Indiana 47907, USA
rklop@purdue.edu, mivantys@purdue.edu

Abstract

Advanced hydrostatic transmissions and hydraulic hybrids show potential in new market segments such as commercial vehicles and passenger cars. Such new applications regard low noise generation as a high priority, thus, demanding new quiet hydrostatic transmission designs. The aim of this paper is to investigate noise sources on a series hybrid transmission through simulation and measurements.

A model has been developed to capture the interaction of a pump and motor working in a hydrostatic transmission and to predict overall noise sources. The model describes dynamics of the system by coupling lumped parameter pump and motor models with a one-dimensional unsteady compressible transmission line model including a dynamic model of an accumulator. A semi-anechoic chamber has been designed and constructed for sound intensity measurements that can be used to derive sound power. Sound power measurements were conducted on a series hybrid transmission test bench inside the semi-anechoic chamber in order to study the relationship between sound power and two types of noise sources, fluid and structure borne. The focus of these measurements was to investigate the impact of an accumulator in the high pressure line as well as the influence of varying high pressure line length.

Results show a strong influence of changing line length and the addition of an accumulator on pressure ripple, but with little impact on sound power. A high correlation was found between sound power levels and control moment amplitudes on the swash plate. This study demonstrates the usefulness of predicting transmission noise sources, and how this information is beneficial in the design process of a transmission.

Keywords: hydrostatic transmission, sound power, noise sources, measurements, TransModel, series hybrid

1 Introduction

More advanced hydrostatic transmission designs, such as the hydraulic series hybrid, are showing potential to be used in new on-road applications such as refuse trucks, buses, delivery trucks and passenger cars. The series hybrid configuration offers energy recovery and improved transmission efficiency compared to conventional mechanical transmissions; however, hydraulic solutions cause an increased risk of noise problems. If not addressed, noise issues may inhibit hydraulic solutions to be used in new on-road applications, especially in the case of passenger cars.

This manuscript was received on 08 April 2011 and was accepted after revision for publication on 30 September 2011

1.1 State of the Art

One of the most common solutions to reduce noise generation in hydraulic systems is to employ passive noise treatment methods. Acoustic enclosures, silencers, vibration mounts, damping treatments and absorbent materials are passive solutions meant to suppress excitation along the noise transmission path. Silencers, for example, are commercially available and target pump-induced harmonic pressure pulsations in an attempt to reduce fluid borne noise. A reactive silencer has been designed by Kojma and Ichiyanagi (2001) and tested in an excavator application. Results illustrated up to 15.1 dB reductions of near-by noise at pump harmonic frequencies. The advantage of passive noise treatments is that they can be applied to an existing system. The primary disadvantage is that noise sources of the system are not targeted. Also, passive techniques require additional components to be added.

Another approach is to focus on sources of excitation. The objective is to minimize oscillating forces and pressure pulsations generated at the pump and motor, thus, reducing vibration of components throughout the system. A key component of axial piston machines is the valve plate. Seeniraj (2009) focused on valve plate design of the pump only and demonstrated up to 5 dBA reductions as a result of reducing the peak-to-peak amplitudes of oscillating swash plate moments and flow ripple. Other techniques such as cross-angle and pre-compression filter volume have been investigated and shown to reduce noise sources, thereby reducing audible noise (Johansson, 2005). Valve plate design has also been investigated focusing on the pump and motor of a hydrostatic transmission (Klop et al., 2007); however, dynamics of pump and motor were captured independently. A comprehensive overview of methods to predict and reduce noise sources of pumps/ motors was done by Edge (1999).

One of the first publications to consider superimposed pressure pulsations between a pump and motor working as a hydrostatic transmission was done by Kojima and Shinada (1986). The four pole transfer matrix approach was applied to the high pressure line and pump and motor source characteristics (source flow and source impedance) were determined by measurements. The advantage of this approach is that solutions of pressure and flow throughout the line are computationally inexpensive and solutions can be obtained at particular frequencies of interest. The disadvantage is that the accuracy of the solution is largely dependent on the accuracy of the pump and motor characteristics derived from measurements. Also, investigation of valve plate design or other design changes within the rotating group would be cumbersome since for each design to be studied, measurements of source characteristics would be necessary.

An alternative modeling approach is to consider a solution in the time domain, in which a one-dimensional distributed line model is coupled with dynamic lumped parameter pump and motor models (Klop, 2010). The advantages are the following: more flexibility to investigate design parameters of the pump and motor, solutions can be obtained without measurements and oscillating forces within the rotating group can be determined providing a prediction of case vibration or structure borne noise. The main disadvantages are that the problem can be mathematically complex, longer simulation time and more difficulty in considering additional components in the line such as silencers, resonators and valves.

Previous studies on noise and vibration reduction specifically of hydraulic hybrids was done by Nguyen (2008) on a parallel hybrid system focusing on effects of magnetorheological (MR) fluids.

One of the main elements that is lacking in previous research is the focus on noise sources of hydrostatic transmissions. The interaction of the pump and motor is critical. A better understanding how to select certain pump/motor combinations, accumulator sizes and locations, line lengths, control strategies and other key design parameters is necessary to create a quiet system. Another missing element in previous research is detailed measurement results of audible noise. In the publications referenced here, sound pressure levels are measured as a means of comparing designs. It remains unclear how changes in noise sources relate to changes of audible noise comparing different systems configurations and pump/motor operating conditions (pressure difference, speeds and displacements). The work presented in this paper attempts to address these missing elements through a detailed study of a series hybrid transmission. Furthermore, the presented work in this paper is step towards a long term goal which is to be able to predict noise sources of a transmission and use this information in the process of designing a quiet system.

1.2 Series Hybrid Transmission

The transmission configuration chosen for the presented research study is a hydraulic series hybrid. An illustration of a simplified circuit is shown in Fig. 1. The chosen vehicle required a 42 cc/rev pump, 75 cc/rev motor and 20L high and low pressure accumulators to be used for a Class I truck delivery application.

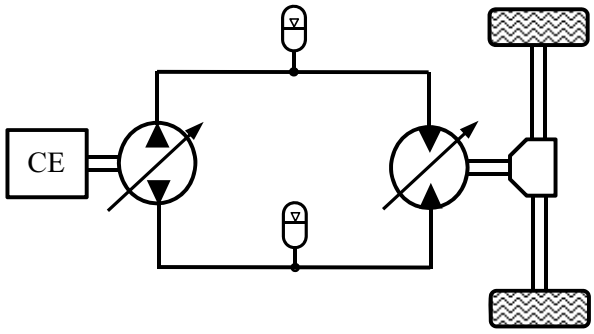

Fig. 1: *Simplified series hybrid transmission*

The goal of the present work is to study noise sources of the pump and motor with respect to sound power. In particular, two key components of the system are investigated: influence of an accumulator in the high pressure line, influence of varying the high pressure line length. The main contributions of the present work are first time sound power measurements of a pump and motor working as a hydrostatic transmission, and a detailed analysis revealing correlations between audible noise, pump/motor operating conditions and system configuration.

2 Noise Sources

In 1976, a massive effort involving four contractors in the United Kingdom over a three year span was conducted to reduce noise in fluid power systems as a whole. One of the results of this work included a clear definition of two noise sources of a pump or motor: Fluid Borne Noise (FBN) and Structure Borne Noise (SBN) (Quieter Fluid Power Handbook, 1982). The contribution of each noise source to audible noise is typically unknown and unique to each particular design; however, previous research demonstrates that

both sources are important to consider and noise reduction can be achieved if both sources are reduced (Klop and Ivantysynova, 2010a).

2.1 Fluid Borne Noise

Fluid borne noise refers to pressure and flow ripples generated by the pump transmitting throughout the hydraulic system inducing vibration of other components and ultimately causing air-borne noise. Figure 2 illustrates an example of the kinematic and real outlet flow ripples of an axial piston machine over one shaft revolution. The real flow ripple includes compressibility effects, which are highly dependent on valve plate geometry, and varying gap flows.

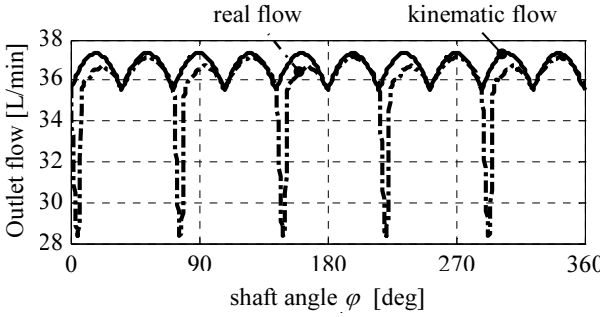

Fig. 2: *Kinematic and real flow ripple for a 5 piston pump*

Typically, FBN of a pump is quantified by peak-to-peak amplitudes of real flow ripple, since information of load dynamics are unknown. In the present work, however, FBN is quantified by peak-to-peak pressure amplitudes as a result of piston frequencies as well as lower frequency system behavior contributions, as shown in Fig. 3. This is made possible by modeling the entire system including dynamics of the pump, motor and connecting high pressure line.

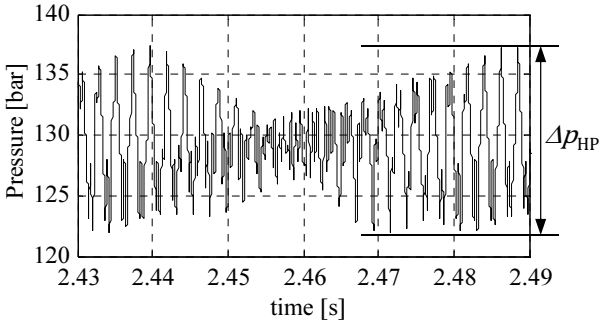

Fig. 3: *Example of pressure at the HP port*

2.2 Structure Borne Noise

Induced vibrations transmitted to the pump casing and further to other connecting components represent a source of structure borne noise. Each piston exerts a force on the swash plate depending on instantaneous cylinder pressure forces, F_{DCi}, piston friction forces, F_{TKi}, and inertia forces, F_{aKi}, as shown in Fig. 4.

These three forces are time dependent and exert a highly oscillating resultant force, F_{NSy}, on the swash plate causing vibration. The resultant force acting in the z direction, F_{rKi}, is described by

$$F_{\mathrm{rKi}} = F_{\mathrm{DCi}} + F_{\mathrm{aKi}} + F_{\mathrm{TKi}} \tag{1}$$

and the component acting perpendicular on the swash plate is therefore

$$F_{\mathrm{NSi}} = \frac{F_{\mathrm{rKi}}}{\cos(\beta)} \tag{2}$$

Figure 4 also illustrates the path of the resultant force for a case with ideal pressure in the displacement chamber (dotted line) as well as real pressure (solid line). Resultant moments acting on the swash plate in x, y and z directions considering the summation of forces from all pistons can be determined.

$$M_{\mathrm{X}} = \frac{R_{\mathrm{b}}}{\cos^2(\beta)} \sum_{\mathrm{i}=1}^{z_{\mathrm{K}}} F_{\mathrm{rKi}} \cos(\varphi_{\mathrm{i}}) \tag{3}$$

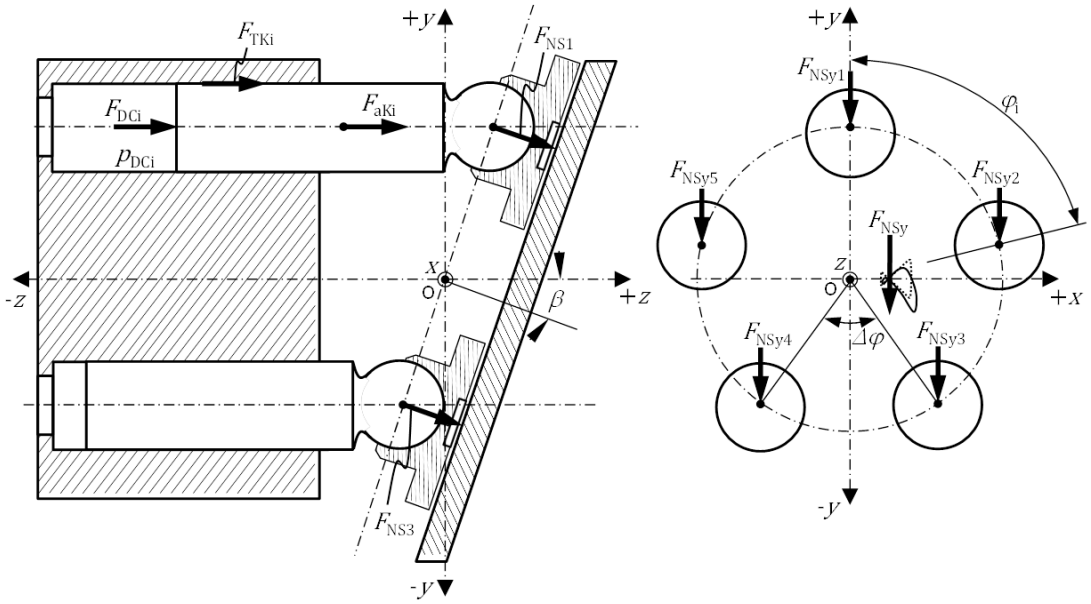

Fig. 4: *Forces acting on the swash plate of a 5 piston pump*

$$M_{\mathrm{Y}} = R_{\mathrm{b}} \sum_{\mathrm{i}=1}^{z_{\mathrm{K}}} F_{\mathrm{rKi}} \sin\left(\varphi_{\mathrm{i}}\right) \tag{4}$$

$$M_{\mathrm{Z}} = -R_{\mathrm{b}} \tan\left(\beta\right) \sum_{\mathrm{i}=1}^{z_{\mathrm{K}}} F_{\mathrm{rKi}} \sin\left(\varphi_{\mathrm{i}}\right) \tag{5}$$

Figure 5 shows an example of calculated swash plate moments. In the present work, SBN is quantified by peak-to-peak amplitudes of all three oscillating moments. Oscillating moments in the x-direction refer to moments acting against the adjustment system.

Moments in the z-direction refer to torque ripple on the shaft, and moments in the y-direction are transferred to the case itself or a bearing.

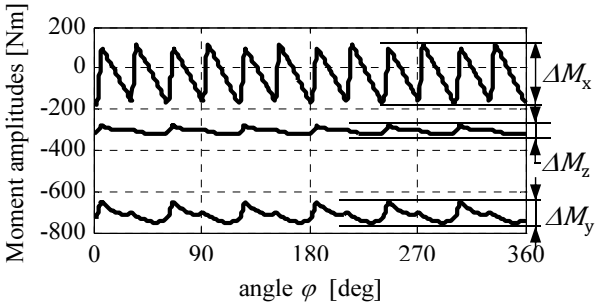

Fig. 5: *Swash plate moments*

3 Transmission Model

This section focuses on a complete model of a hydrostatic transmission solved in the time domain. Four sub-sections are written describing each component of the complete model: pump/motor model, transmission line model, friction model, and accumulator model.

3.1 Pump/Motor

The method for modeling flow through a pump and motor resembles that by Wieczorek and Ivantysynova (2000) based on a lumped parameter approach. Regarding both sources of noise, the most critical parameter to predict is pressure in the displacement chamber. This is achieved by considering a control volume of each displacement chamber and solving a set of pressure build-up equations derived from continuity and the definition of bulk modulus. Figure 6 illustrates the control volume of one displacement chamber with all in/out flows.

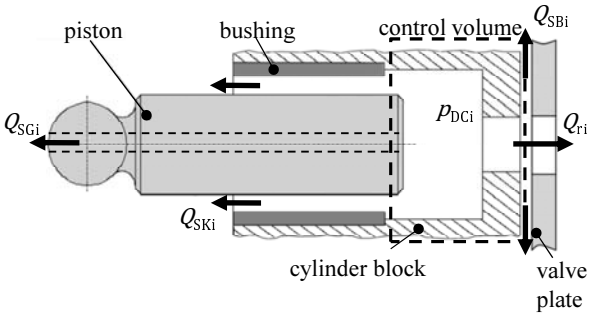

Fig. 6: *Displacement chamber control volume*

The pressure build-up equation is written based on volumetric flows through the piston/cylinder gap, Q_{SKi}, slipper/swash plate gap, Q_{SGi}, and cylinder block/valve plate gap, Q_{SBi}.

$$\frac{dp_{\mathrm{DCi}}}{dt} = \frac{K}{V_{\mathrm{i}}}\left(Q_{\mathrm{ri}} - Q_{\mathrm{SKi}} - Q_{\mathrm{SGi}} - Q_{\mathrm{SBi}} - \frac{dV_{\mathrm{i}}}{dt}\right) \tag{6}$$

Figure 7 illustrates the position of one displacement chamber control volume at ODC open to both ports. Flow entering/exiting the chamber into high pressure and/or low pressure ports is denoted by Q_{ri}, which is calculated based on the orifice equation.

$$Q_{\mathrm{rHPi}} = \alpha_{\mathrm{HP}} A_{\mathrm{rHPi}} \sqrt{\frac{2}{\rho_{\mathrm{HP}}}} \sqrt{\left|p_{\mathrm{DCi}} - p_{\mathrm{HP}}\right|} \operatorname{sgn}\left(p_{\mathrm{HP}} - p_{\mathrm{DCi}}\right) \tag{7}$$

$$Q_{\mathrm{rLPi}} = \alpha_{\mathrm{LP}} A_{\mathrm{rLPi}} \sqrt{\frac{2}{\rho_{\mathrm{LP}}}} \sqrt{\left|p_{\mathrm{DCi}} - p_{\mathrm{LP}}\right|} \operatorname{sgn}\left(p_{\mathrm{LP}} - p_{\mathrm{DCi}}\right) \tag{8}$$

$$Q_{\mathrm{ri}} = Q_{\mathrm{rHPi}} + Q_{\mathrm{rLPi}} \tag{9}$$

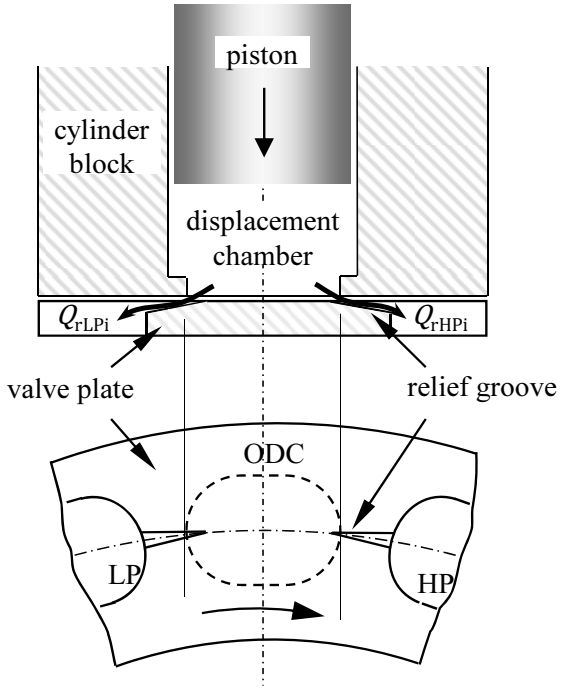

Fig. 7: *Flow through valve plate*

The change in volume of the displacement chamber throughout one shaft revolution is dependent on pump kinematics and can be calculated by

$$\frac{dV_{\mathrm{i}}}{dt} = v_{\mathrm{Ki}} A_{\mathrm{Ki}} \tag{10}$$

where v_{Ki} and A_{Ki} represent piston velocity and piston area, respectively. Two other pressure build-up equations are written, one for low pressure port and one for high pressure port. Figure 8 illustrates the control volume for the high pressure port and flows entering and exiting.

Pressure build-up equations for the LP and HP port are as follows.

$$\frac{dp_{\mathrm{LPp}}}{dt} = \frac{K}{V_{\mathrm{LPp}}}\left(\sum_{\mathrm{i}=1}^{z} Q_{\mathrm{IN}} - Q_{\mathrm{rLPpi}}\right) \tag{11}$$

$$\frac{dp_{\mathrm{HPp}}}{dt} = \frac{K}{V_{\mathrm{HPp}}}\left(\sum_{\mathrm{i}=1}^{z} Q_{\mathrm{rHPpi}} - Q_{0}\right) \tag{12}$$

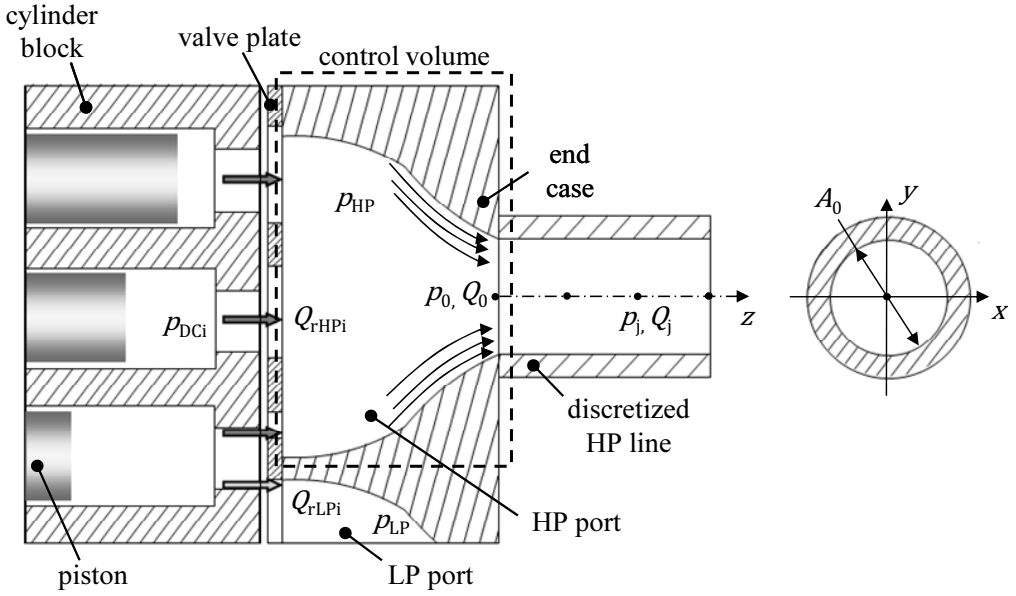

Fig. 8: *High pressure port control volume*

Flow, Q_{IN}, represents flow entering the low pressure port volume of the pump which is determined based on area opening A_{IN} and boundary pressure p_{IN}, as shown in Fig. 9.

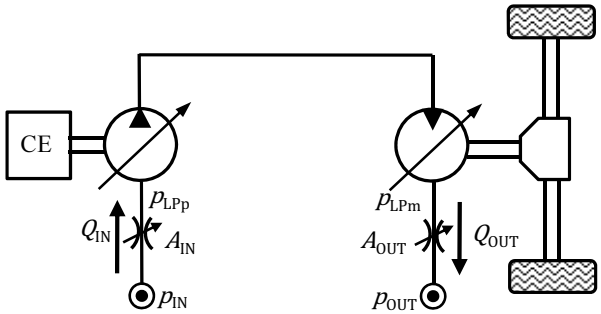

Fig. 9: *Pump inlet and motor outlet boundaries*

This model does not characterize flow in the low pressure line of the transmission. Instead, boundary pressures and throttle openings are set as constants to achieve desired low pressures of the system. This is a reasonable assumption regarding noise source prediction because most of the energy causing vibration is due to high pressure oscillations. Flow entering the low pressure port of the pump and exiting the low pressure port of the motor is calculated as follows

$$Q_{IN} = \alpha A_{IN} \sqrt{\frac{2}{\rho_{LPp}}} \sqrt{\left|p_{IN} - p_{LPp}\right|} \operatorname{sgn}\left(p_{IN} - p_{LPp}\right) \quad (13)$$

$$Q_{OUT} = \alpha A_{OUT} \sqrt{\frac{2}{\rho_{LPm}}} \sqrt{\left|p_{LPm} - p_{OUT}\right|} \operatorname{sgn}\left(p_{LPm} - p_{out}\right) \quad (14)$$

Flow exiting the pump HP port, Q_0, can be determined by solving a momentum equation capturing fluid acceleration from the valve plate to the outlet port due to changing cross sectional area. A linear momentum equation is written for a fixed control volume in the direction of the line, as shown in Fig. 8. The momentum equation can be expressed as follows.

$$\vec{F}_{FMIN} - \vec{F}_{FMOUT} + \left[\vec{F}_{perm} + \vec{F}_{imperm}\right] = \frac{\partial}{\partial t}\left(\int_V \rho \vec{v} dV\right) \quad (15)$$

The first and second terms of Eq. 15 are the flux of momentum entering and exiting the volume, respectively. The term in brackets represents the sum of the forces acting on the fluid during the time interval *dt*. The right-hand side represents change of momentum during the same time interval. Equation 15 can be simplified to a form where the change in fluid velocity at the exit of the HP port is described. Velocity v_0 serves as a boundary condition for the line coupling the lumped parameter pump model with the distributed parameter line model. Details of this derivation can be found in Klop (2010b).

$$\frac{dv_0}{dt} = \frac{1}{V_{HP}\rho_{HP}}\left[\vec{F}_{FMIN} - \vec{F}_{FMOUT} + \vec{F}_{perm} + \vec{F}_{imperm}\right] - \frac{1}{\rho_{HP}} \frac{\frac{dp_{HP}}{dt}}{\frac{dp_{HP}}{d\rho_{HP}}} v_0 \quad (16)$$

In summary, the total number of differential equations solved in the dynamic pump model is equal to the number of pistons plus three, two for the high and low pressure ports, and one for the velocity exiting the pump. For example, a five piston pump would require 8 ODE's to be solved simultaneously; this can be achieved using a standard numerical technique, 6th order Runge-Kutte method. An open source code written by Ashby (2002) was used to solve a system of ordinary differential equations.

For the dynamic motor model, identical equations of the pump model are solved, but with flow in the opposite direction and one additional ODE. An additional dynamic equation is needed to calculate speed of the motor. Motor angular speed, ω_m, is not a constant set by the user as in the case with the pump; instead, it is calculated dependant on a load torque, M_{Load}, on the output shaft and torque generated by the motor itself, M_{zm}.

$$\frac{d\omega_{\mathrm{m}}}{dt}=\frac{1}{l_{\mathrm{m}}}\left[-M_{\mathrm{zm}}\left(\omega_{\mathrm{m}}\right)-M_{\mathrm{Load}}-M_{\mathrm{Loss}}\right] \tag{17}$$

In this way, pressure in the high pressure line can be set to a desired pressure by adjusting a constant load torque.

3.2 Method of Characteristics Line Model

The line model solves one dimensional unsteady compressible flow through a straight pipe; the approach is based on that described by Wylie and Streeter (1978). Two quasi-steady hyperbolic differential equations based on conservation of fluid flow momentum and continuity through a constant diameter pipe are

$$\frac{1\partial p}{\rho\partial z}+\frac{\partial v}{\partial t}+\frac{2}{\rho R}\tau=0 \tag{18}$$

$$\frac{\partial p}{\partial t}+\rho c^{2}\frac{\partial v}{\partial z}=0 \tag{19}$$

where p indicates pressure, v represents the fluid velocity in the direction of the pipe or z direction, D is the pipe diameter, c is wave speed and τ describes wall shear stress, which can be divided into steady or unsteady components. Wave speed is determined based on fluid bulk modulus, K, Young's modulus of the pipe wall, E, and wall thickness, e.

$$c=\frac{\sqrt{\frac{K}{\rho}}}{\sqrt{1+\frac{KD}{Ee}}} \tag{20}$$

This pair of hyperbolic partial differential equations is not solved directly; however, they are transformed by method of characteristics into four ordinary differential equations. Given a set of ordinary differential equations, finite difference approximations can be used to set up a solvable system of equations

$$C^{+}:\ p_{\mathrm{Nj}}=C_{\mathrm{p}}-B_{\mathrm{L}}Q_{\mathrm{Nj}} \tag{21}$$

$$C^{-}:\ p_{\mathrm{Nj}}=C_{\mathrm{m}}+B_{\mathrm{L}}Q_{\mathrm{Nj}} \tag{22}$$

where C_{p}, C_{m}, and B_{L} are defined as

$$C_{\mathrm{p}}=p_{\mathrm{j\text{-}1}}+B_{\mathrm{L}}Q_{\mathrm{j\text{-}1}}-\frac{2\Delta z}{R}\tau_{\mathrm{j\text{-}1}} \tag{23}$$

$$C_{\mathrm{m}}=p_{\mathrm{j+1}}-B_{\mathrm{L}}Q_{\mathrm{j+1}}+\frac{2\Delta z}{R}\tau_{\mathrm{j+1}} \tag{24}$$

$$B_{\mathrm{L}}=\frac{\rho c}{A_{\mathrm{L}}} \tag{25}$$

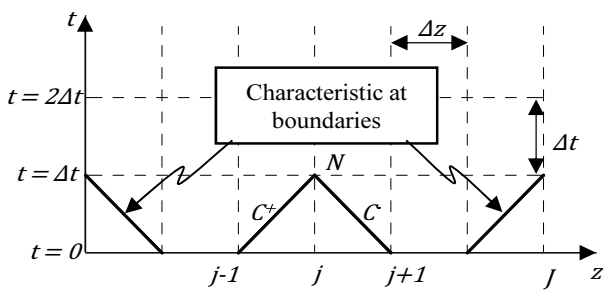

Fig. 10: *One dimensional line grid arrangement*

As shown in Fig. 10, the set of C^{+} and C^{-} equations represent characteristic lines in the + z and - z directions, respectively. Note that subscript N represents a quantity at the next time step. More details can be found in the following section concerning the calculation of τ.

Given initial conditions at time zero, pressures and flows at all inner nodes can be determined directly by solving Eq. 21 and 22 for Q_{Nj} and p_{Nj} simultaneously. At nodes $j = 0$ and $j = J$, necessary boundary conditions dictate characteristic equations. At the pump outlet, a flow boundary is forced as a result of pump dynamics; therefore, only pressure is calculated with the line model using Eq. 22 and assuming $Q_{\mathrm{N0}} = Q_0$. Note that an iteration process is necessary to solve for pressure and flow at the first node of the next time step. This is because pressure at the first node is a boundary for the dynamic pump model, and flow is a boundary for the line model. In this particular case, given a sufficiently small time step in the solver, only two or three iterations are needed for convergence. The boundary of the motor, $j = J$, is also a forced flow boundary. The iteration process described also applies to the motor.

3.3 Friction Model

The friction model of flow in the high pressure line is divided into two components: steady and unsteady. Steady friction loss is described based only on the instantaneous mean velocity of the fluid, v_{j}, and calculated as

$$\tau_{\mathrm{steady,j}}=\frac{1}{8}\rho f_{\mathrm{j}}v_{\mathrm{j}}\left|v_{\mathrm{j}}\right| \tag{26}$$

where f_{j} denotes the Darcy-Weisbach friction factor at node j. The Darcy-Weisbach friction factor can be calculated based on empirical data for laminar and turbulent flow (Munson et al., 2002).

$$f_{\mathrm{laminar,j}}=\frac{64}{\mathrm{Re}_{j}} \tag{27}$$

$$f_{\mathrm{turbulent,j}}=\frac{0.316}{\mathrm{Re}_{j}^{0.25}} \tag{28}$$

Unsteady friction for laminar flow is determined based on an approximation method developed by Schohl (1993); this method estimates the influence of frequency dependent friction (FDF). The unsteady component is calculated by

$$\tau_{\mathrm{unsteady,j}}=\frac{2\rho v_{\mathrm{j}}}{R}\sum_{\mathrm{i}=1}^{\mathrm{S}}m_{\mathrm{i}}y_{\mathrm{ij}} \tag{29}$$

where m_{i} is a series of coefficients [1.051, 2.358, 9.021, 29.47,79.55]. The second term inside the summation, $y_{\mathrm{ij}}(t)$, is an updated value representing change in velocity at previous time steps. At the first time step, $y_{\mathrm{ij}}(0) = 0$. At each subsequent time step, the values for $y_{\mathrm{ij}}(t)$ are updated based on 5 previous values of instantaneous velocity at point j.

$$y_{\mathrm{ij}}\left(t+\Delta t\right)=e^{-\mathrm{ni}\Delta t/\mathrm{T}}\,y_{\mathrm{ij}}\left(t\right)+\Delta y_{\mathrm{ij}}\left(t\right) \tag{30}$$

$$\Delta y_{ij}(t) = \frac{\left(1 - e^{-ni\Delta t/T}\right)}{n_i \frac{\Delta t}{T}} \left[v_j(t + \Delta t) - v_j(t) \right] \tag{31}$$

$$T = \frac{D^2}{4\upsilon} \tag{32}$$

The term in the exponential, n_i, is also a series of coefficients [26.65, 100, 669.6, 6497,57990].

3.4 Bladder Type Accumulator Model

A model of a bladder type accumulator has been implemented in order to study its effect on noise sources. This model is based on that proposed by Wylie and Streeter (1978) where a set of five non-linear equations are solved simultaneously.

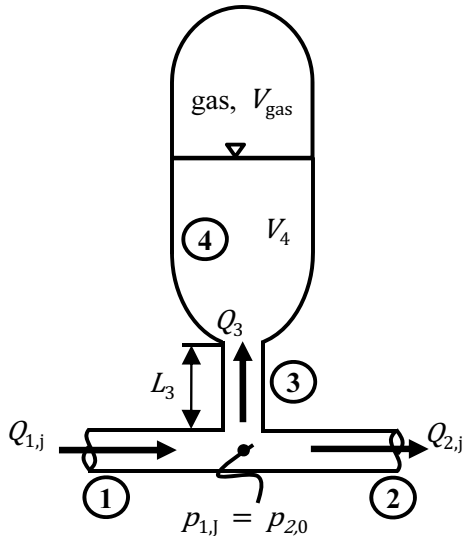

Fig. 11: *Bladder type accumulator model factors*

Figure 11 illustrates a picture of a bladder type accumulator with four different sections labeled: (1) line connecting to the accumulator from the source of flow, (2) line connecting after the accumulator, (3) short line connecting main line with accumulator, (4) fluid inside the accumulator. At the junction of (1), (2), and (3), a continuity equation can be written

$$Q_{N1,J} = Q_{N2,0} + Q_{N3} \tag{33}$$

where J represents the last node of line (1) and N indicates the next time step.

Flow entering or exiting the accumulator through line (3) is assumed as a lumped inelastic and incompressible volume of fluid where inertia and friction effects are considered. The equation of motion leads to the following relationship.

$$p_{N1,J} - p_{N4} = C_1 + C_2 Q_{N3} \tag{34}$$

$$C_1 = p_4 - p_{1,J} + \frac{f_3 L_3 \rho}{D_3 A_3} Q_3 \left| Q_3 \right| - C_2 Q_3 \tag{35}$$

$$C_2 = \frac{2L_2}{g A_2 \Delta t} \tag{36}$$

where D_2, A_3, and L_3 represent the diameter, area opening, and length of line (3), respectively. The relationship between the fluid in the accumulator and the volume of the air can be expressed as a polytropic process.

$$p_{N4}\left(V_{gas} - \frac{(Q_{N3} + Q_3)}{2} \Delta t \right) = C \tag{37}$$

For this particular application, the process is considered to be adiabatic since the volumes are relatively small and the response time of the accumulator is fast. Finally, two more equations can be written providing a relationship between $Q_{N1,J}$ and $Q_{N2,0}$ by using compatibility equations described by Eq. 21 and 22. A total of five equations can be solved simultaneously at each time step for 5 unknowns: $Q_{N1,J}$, $Q_{N2,0}$, $p_{N1,J}$, p_{N4}, Q_{N3}. This is done using Newton's method; a small time step (< 1 μs) generally requires two or three iterations before finding a solution. The accumulator model has also been implemented as an optional component of the complete transmission model.

3.5 Model Validation

Validation of the transmission model has been accomplished in several stages based on measurements of dynamic pressure in the high pressure line and displacement chamber. Refer to Klop and Ivantysynova (2009), Klop and Ivantysynova (2010b) and Klop (2010) for details.

4 Test rig Setup

A series hybrid transmission test rig was built with capabilities of measuring pressure ripple and sound power of the pump and motor. The hydraulic schematic is illustrated in Fig. 12. This test setup was built inside a semi-anechoic chamber such that the transmission was in the acoustic measurement area, and the electric drive and generator were excluded by a thick-walled barrier. Sound power level (SWL) measurements were conducted in accordance to ISO 16902-1.

The measured signals of primary interest were two dynamic pressures in the HP line as shown in Fig. 12: p_{HP1} and p_{HP3}. Kistler type 603B1 pressure transducers were used with a range of 0 - 1000 bar, 1.1 % accuracy and 500 kHz resonant frequency. Pressure signals p_{HP1} and p_{HP3} are as close as possible to the HP ports of the pump and motor, respectively. These locations were chosen in an attempt to closely reflect resultant forces acting on the units as a result of the standing wave in the HP line, thus audible noise. The accumulator is mounted 2.39 m from the pump outlet.

Measurements were conducted with four different system arrangements: accumulator and line length L_1 = 4.81 m, accumulator and line length L_2 = 5.78 m, no accumulator and line length L_1, no accumulator and line length L_2. The additional line length was added between the junction at the accumulator and the motor inlet.

This test rig was controlled using an XPC-Target system in a Matlab/Simulink environment and was controlled in two different modes of operation: Hybrid system configuration with the HP accumulator connected, Standard hydrostatic transmission without the HP accumulator.

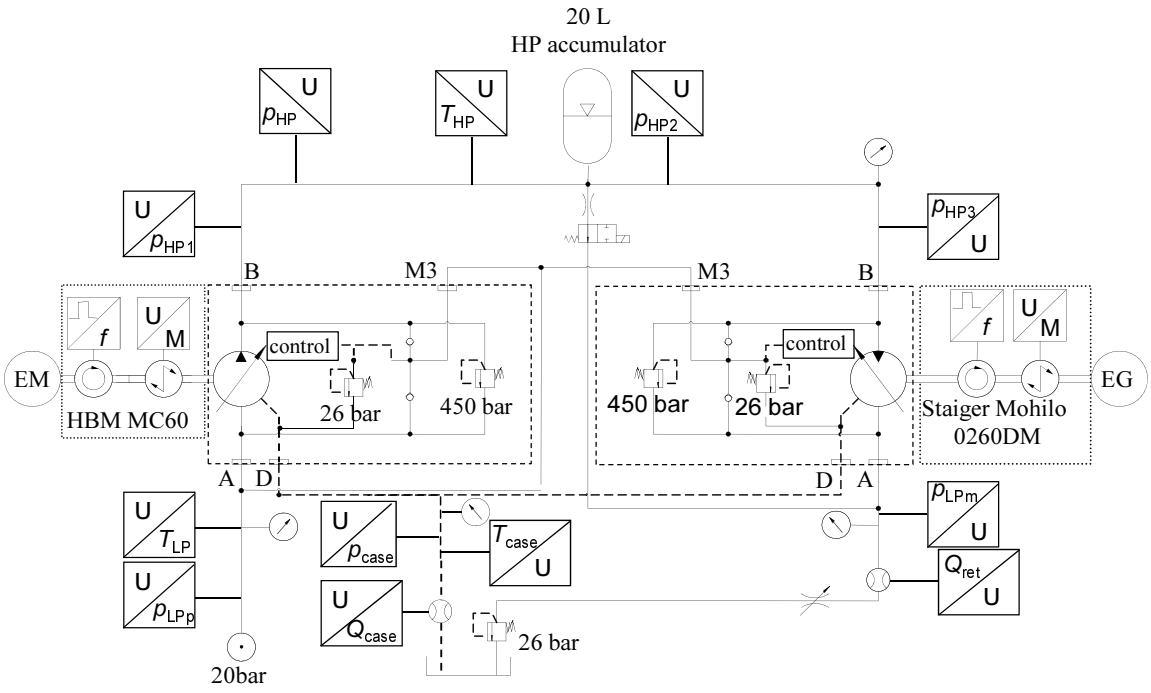

Fig. 12: *Hydraulic schematic of test rig*

Hybrid system configuration

The speed of the electric motor and generator used as drive and load units of the transmission were controlled using closed-loop speed control. For control of the pressure of the hybrid system, the pump displacement was controlled by implementing a closed-loop pressure control. The displacement of the motor was in open-loop electro-hydraulic control and carefully adjusted at each operating point to achieve a desired torque. Low pressures of both units were maintained to be 20 bar, and inlet temperature was held at 52 ± 1°C.

Standard hydrostatic transmission

The electric motor used as a drive unit runs in speed-control mode and the electric generator used a load unit runs in closed-loop torque control. Displacements of the pumping and motoring units were both in open-loop electro-hydraulic control. Displacements were initialized to 0 % at each operating point and carefully adjusted to achieve desired motor speeds and torques. Low pressures of both units were maintained to be 20 bar, and inlet temperature was held at 52 ± 1°C.

5 Measurement Results and Discussion

Measurements were conducted for four different system arrangements and three different operating conditions, see Table 1. Test number T1 is an operating point at low vehicle speed and high load torque representing a moment where the vehicle is climbing a grade. Test number T2 represents a condition where the vehicle is at a relatively low speed and cruising; this is a point that is very often reached in a typical drive cycle. Test number T3 is a condition at the maximum speed of the vehicle; the main purpose of this operating point is to study noise sources when the pump is at full displacement.

Table 1: Tested operating conditions

			Test number		
System Parameter	Symbol	Unit	T1	T2	T3
Vehicle Speed	v_{veh}	km/hr	24	56	104
Pump speed	n_p	rpm	2000	2000	3000
Pump displacement	β_p	%	78.9	72.6	100
Pump power	P_p	kW	24	17	44
Motor speed	n_m	rpm	731	1706	3167
Motor displacement	β_m	%	100	38.5	48.2
Motor power	P_m	kW	20	14	40
Load torque	M_{Load}	Nm	248	65	100
High pressure	p_{HP}	bar	239	189	232
Low pressure	p_{LP}	bar	20	20	20

At each operating condition and system configuration, measurements of pressure ripple and sound power were conducted. Pressure ripple measurements provide a quantification of fluid borne noise and structure

borne noise is quantified from simulated swash plate moments based on the model described in section 3 and equations in section 2. The objective of these measurements is to compare both sources of noise with sound power studying the influence of line length and effects of including an accumulator.

5.1 Influence of Line Length

Line length is a critical parameter which dictates timing of superimposed pump and motor induced harmonic pressure oscillations. These measurements reveal not only the impact of varying line length on pressure pulsations in the line, but also how these impacts relate to audible noise.

An example showing the impact of line length on pressure ripple is shown in Fig. 13 with measurements taken on the hybrid configuration at test number T2.

Measurements at the HP port of the motor illustrate decreased pressure ripple from 23.26 to 13.5 bar comparing L_1 = 4.81 m and L_2 = 5.78 m, respectively; this is a reduction of 41.9 %. Also plotted in Fig. 13 are amplitudes of pump and motor harmonics in the frequency domain. It is clear that the most contribution of pressure ripple reduction is at the first harmonic of the pump (the second data point at 300 Hz) and slight increases are found at higher frequencies. This is an example showing the impact of line length where energy is broadened over the frequency spectrum.

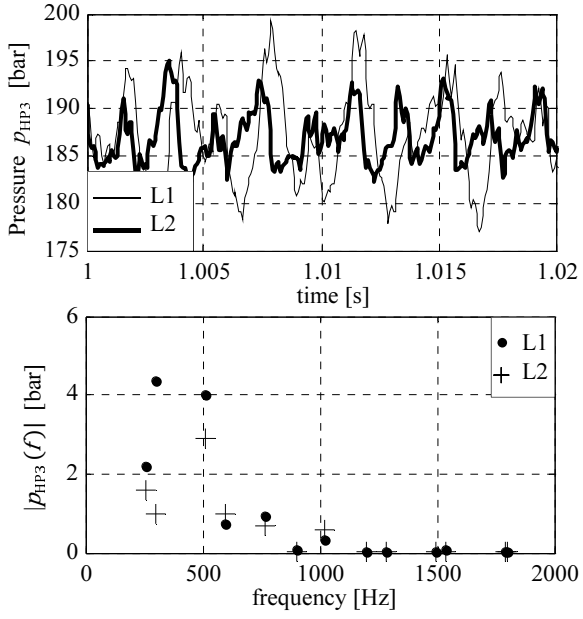

Fig. 13: *Simulated pressure for L1 and L2 at sensor location 3 for test number T2 with hybrid system configuration (n_p = 2000 rpm, β_p = 72.6 %, n_m = 1706 pm, β_m = 38.5 %)*

Figure 14 illustrates measured sound power, measured FBN source (Δp_{HP}) and simulated SBN sources (ΔM_x, ΔM_y, ΔM_z) of the pump with the hybrid system (including accumulator) comparing line lengths L_1 and L_2. All data for L_1 is plotted as bars and all data for the L_2 is plotted using markers for each operating condition. For the system with line length L1, measured sound power levels for T1, T2 and T3 were 96.2, 94.8 and 98.9 dBA, respectively. This trend of SWL correlates with pump power (see Table 1). In other words, the total sound power of the unit is dictated by the magnitude of power generated by the unit.

Also it is interesting to note that swash plate moments follow the trend of pump power, while pressure ripple at the HP port does not. For example by comparing results at test number T2 and T1 for the system with line length L_1, pressure amplitude, Δp_{HP}, slightly increased (16 %), going against the trend of SWL and pump power. On the other hand swash plate moment amplitudes, especially ΔM_x, decreased (21.8 %), which follows the trend of pump power and resulted in lower sound power radiation. The same result is apparent for line length L_2. These results illustrate that for this system and these particular conditions, SWL for the pumping unit correlates more with SBN sources.

By comparing results of L_1 and L_2 in Fig. 14, it is interesting to notice that SWL does not change significantly despite relatively large differences in Δp_{HP} and ΔM_y. The largest change in SWL is observed at T2 (0.5 dBA). One explanation is that ΔM_x, which is the most oscillatory and generally considered to contribute towards SWL the most, was not significantly impacted due to changing line lengths in this case.

In fact, trends of SWL and ΔM_x comparing L_1 and L_2 are very closely matching compared to other noise sources. In particular, slight decreases in ΔM_x correspond to slight decreases in SWL for all operating conditions. These results also support the previous finding that ΔM_x correlates the most with SWL.

Figure 15 illustrates identical comparisons as shown in Fig. 14, but for the motor. In this case, sound power levels increase considerably from T1, T2 and T3 which, unlike the pump, does not correlate with hydraulic power. Clearly, SWL for the motor is dictated by the speed of the unit. Pressure ripple amplitudes also follow the trend of SWL whereas moment amplitudes are opposite. Moment amplitudes are largest at T1 because the displacement is 100 % where for T2 and T3, the motor displacement is significantly lower (38.5 48.2 %). Despite such large moment amplitudes at T1, results indicate that SWL is more influenced by motor speed.

Regarding the impact of changing line length from L_1 to L_2, nearly all sources were reduced using line length L_2; however, sound power levels did not change significantly. The largest impact on SWL occurred at test number T1 (1.0 dBA). At test number T3 the sound power did not change at all despite large reductions of Δp_{HP}, ΔM_y and ΔM_z. Another trend that can be observed from Fig. 15 is high correlation between SWL and ΔM_x with respect to line length. More specifically, SWL and ΔM_x slightly decrease at test numbers T1 and T2, while SWL and ΔM_x slightly increase at T3.

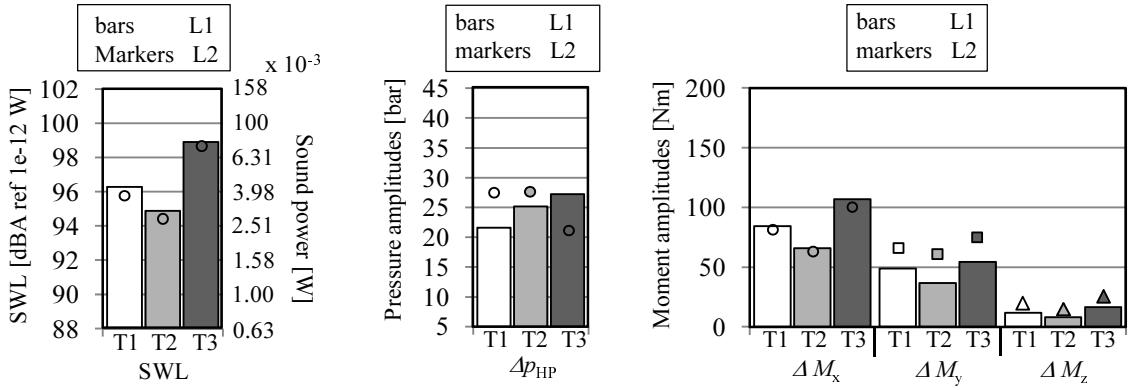

Fig. 14: *Measured SWL, measured FBN sources and simulated SBN sources on hybrid system for the pump. Results of L1 = 4.81 m (bars) and L2 = 5.78 (markers) are plotted for each operating condition*

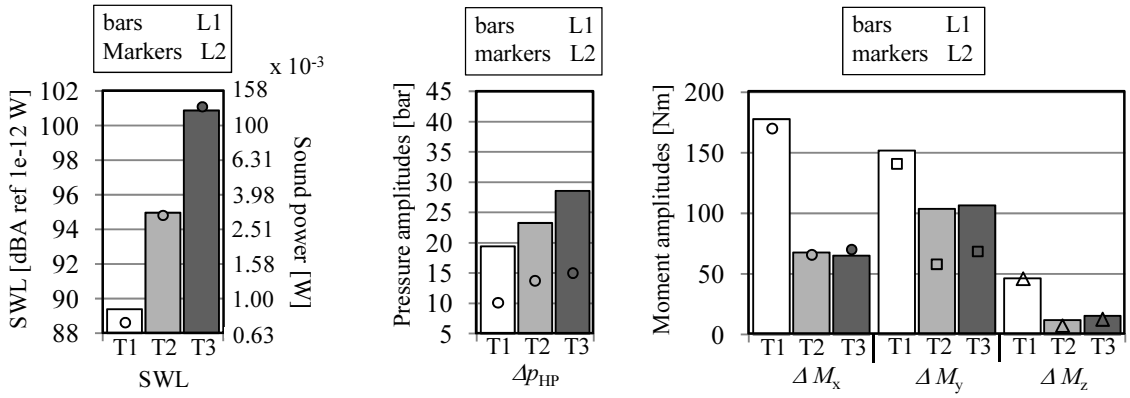

Fig. 15: *Measured SWL, measured FBN sources and simulated SBN sources on the hybrid system for the motor. Results of L1 = 4.81 m (bars) and L2 = 5.78 (markers) are plotted for each operating condition*

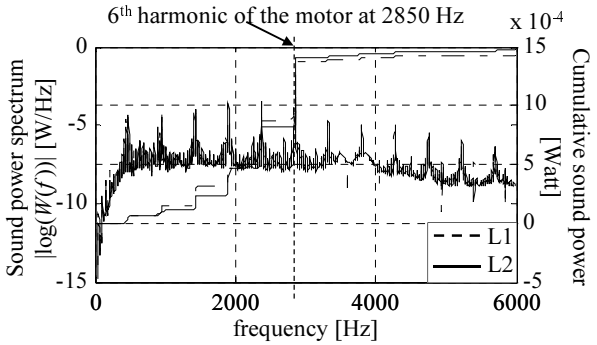

Fig. 16: *Sound power spectrum and cumulative sound power for the motor with the hybrid system configuration at test number T3 for L1 (dotted) and L2 (solid)*

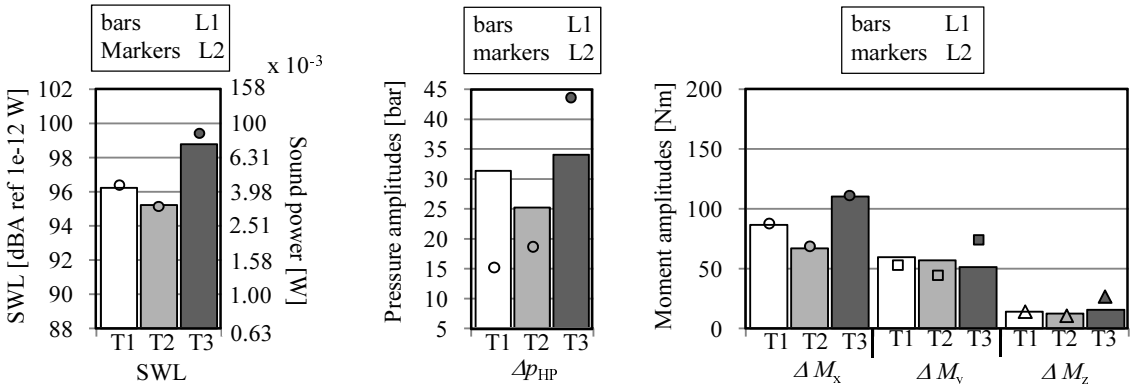

Fig. 17: *Measured SWL, measured FBN sources and simulated SBN sources on the non-hybrid system for the pump. Results of L1 = 4.81 m (bars) and L2 = 5.78 (markers) are plotted for each operating condition*

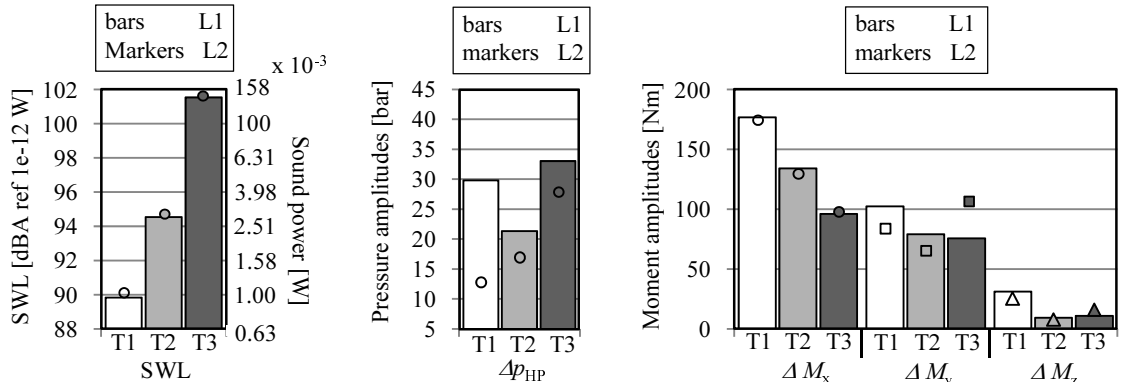

Fig. 18: *Measured SWL, measured FBN sources and simulated SBN sources on the non-hybrid system for the motor. Results of L1 = 4.81 m (bars) and L2 = 5.78 (markers) are plotted for each operating condition*

Although, it may appear that reductions of Δp_{HP}, ΔM_y and ΔM_z had no effect on sound radiation (Fig. 15), a closer look at the sound power spectrum reveals differences at particular frequency ranges. Figure 16 illustrates the sound power spectrum and cumulative sound power of the motor at test number T3 of Fig. 15 for line lengths L_1 and L_2. In this representation of sound power as a function of frequency, it is observed that varying line length from L_1 to L_2 reduced sound power below 2850 Hz, but increased sound power above 2850 Hz. The overall sound power level turns out to be unchanged comparing L_1 and L_2. This result indicates that higher frequency components can also play a role despite not impacting pressure and moment peak-to-peak amplitudes.

Figure 17 and 18 illustrate the same comparisons as Fig. 15 and 14 but for the non-hybrid system without an accumulator in the HP line. The trends of SWL and noise sources with respect to changing line length are very similar. In particular, sound power levels do not change significantly due to varying line length despite large impacts on pressure ripple. It is observed for the pump (Fig. 17) and motor (Fig. 18) that the lack of change in ΔM_x results in unchanging SWL.

Based on all results illustrating the impact of line length, it can be concluded that for this particular transmission with these units, the impact of line length is marginal with respect to noise generation. It has been shown that varying line length significantly impacts pressure ripple in the HP line as well as moment amplitudes ΔM_y and ΔM_z. However, as indicated with acoustic measurements, the swash plate moment amplitude in the x direction appears to have the highest correlation with sound power. A more complete analysis that may be considered in the future would be to measure sound power levels where ΔM_x is varied; this could be accomplished by repeating measurements for a different valve plate.

5.2 Influence of Accumulator

The addition of a HP accumulator in the hybrid system configuration offers similar benefits as a Helmholtz resonator. Figure 19 illustrates typical transmission loss (TL) behavior where a peak occurs at the natural frequency of the resonator, f_n, and TL quickly dissipates away from f_n.

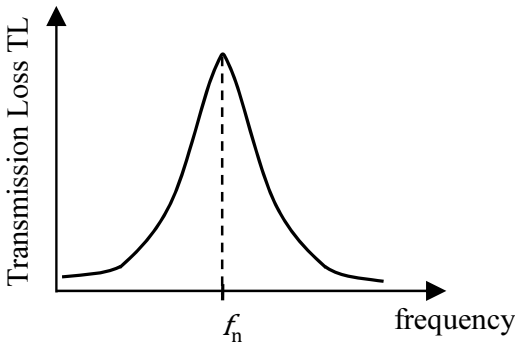

Fig. 19: *Transmission loss of a typical HP accumulator*

The natural frequency of the accumulator can be calculated by

$$f_n = c\sqrt{\frac{A_3}{L_3 V_{tot}}} \tag{38}$$

where c is wave speed, A_2 and L_2 represent the area and length of the neck, respectively, and V_{tot} is the total volume of the accumulator (Quieter Fluid Power Handbook, 1982). In this particular study, values for A_3, L_3, and V_{tot} are 1.11E-3 m^2 (D_2 = 3.81 cm (1.5 in.)), 0.3655 m, and 20 L, respectively. Wave speed was taken as constant (c = 1090 m/s) in all simulations. Solving for the natural frequency of the accumulator results in f_n = 430 Hz. Therefore, it is expected that the largest reductions in pressure ripple will be exhibited at test number T3, since at T3, the pump fundamental frequency is 450 Hz (n_p = 3000 rpm).

The same data presented in the previous section is plotted in Fig. 20 and 21 with the focus of comparing the hybrid system with the non-hybrid system in order to investigate the influence on an accumulator. Since line length L_2 led to mostly less noise sources considering all tested operating conditions compared to L_1, comparison of hybrid and non-hybrid systems are made with L_2 only. Figure 20 illustrates measured sound power, measured FBN source (Δp_{HP}) and simulated SBN sources (ΔM_x, ΔM_y, ΔM_z) of the pump with line length L_2 comparing hybrid and non-hybrid system configurations. All data for the hybrid system with an accumulator is plotted as bars and all data for the non-hybrid system is plotted using markers for each operating condition.

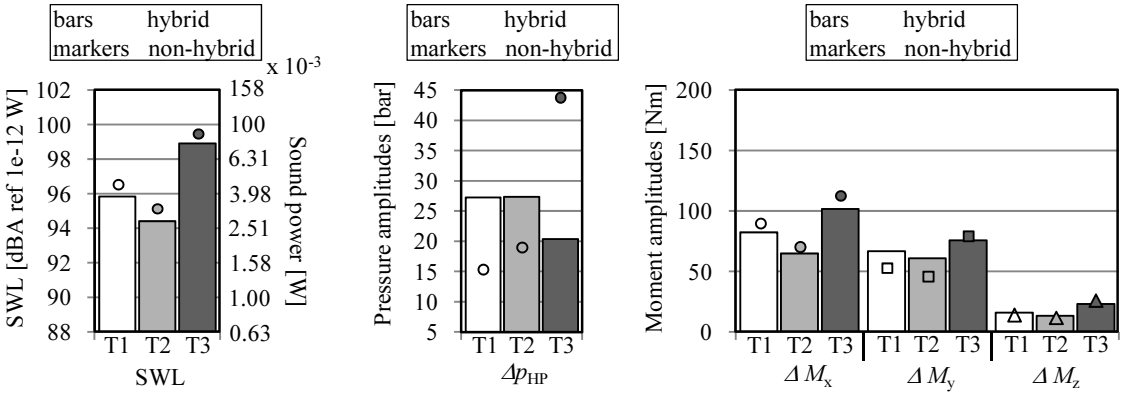

Fig. 20: *Measured SWL, measured FBN sources and simulated SBN sources for the pump and line length L2. Results of the hybrid (bars) and non-hybrid system configuration are plotted for each operating condition*

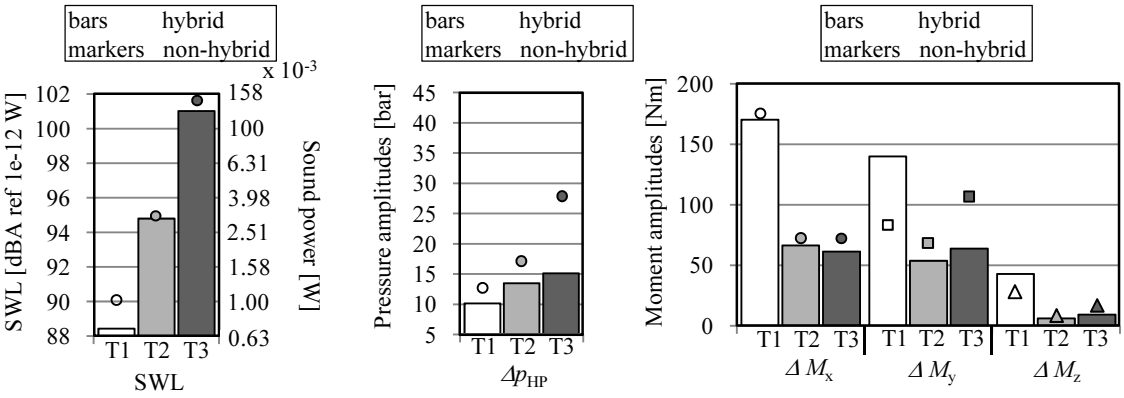

Fig. 21: *Measured SWL, measured FBN sources and simulated SBN sources for the motor and line length L2. Results of the hybrid (bars) and non-hybrid system configuration are plotted for each operating condition*

Firstly, the accumulator was observed to have a significant impact on pressure ripple. At test numbers T1 and T2, the addition of the accumulator resulted in higher pressure ripple at the pump HP port (43.4 % and 32.4 %), while at T3, pressure ripple was significantly reduced (54 %). Such a reduction of pressure ripple at test number T3 was expected as explained previously.

By comparing results of sound power, it appears that an addition of an accumulator does not result in significant change in SWL of the pump. The largest change in SWL occurred at T2 (0.75 dBA), see Fig. 20. It is interesting to observe that for all test numbers, SWL decreased with the hybrid system. Also, changes in SWL correspond with changes in ΔM_x, as opposed to pressure ripple and other noise sources. This result also supports the finding that ΔM_x has the largest correlation to sound power for this particular transmission.

Figure 21 illustrates results similar to Fig. 20 but for the motor. The addition of an accumulator resulted in lower pressure ripple at the HP port for all test conditions; the largest reductions are observed at T3 (46%), which is expected. Results of SWL reveal the largest difference, comparing the hybrid and non-hybrid systems, was at test number T1 (1.8 dBA). In this case, the hybrid configuration was found to exhibit reductions of all noise sources with two exceptions (ΔM_y and ΔM_z at test number T1) and consequently, reductions in sound power.

6 Conclusion

The aim of this paper was to study noise sources of the pump and motor with respect to sound power and in particular, two key components of the system were investigated: influence of an accumulator in the high pressure line, influence of varying the high pressure line length. A series hybrid transmission test rig was built allowing measurements of pressure ripple at the HP ports of both units to be used as a quantity of FBN. The test rig was built inside a semi-anechoic chamber allowing sound power measurements of the pump and motor. A proposed model describes dynamics of the system by coupling lumped parameter pump and motor models with a one-dimensional transmission line model including a dynamic model of an accumulator. The model was used to evaluate peak-to-peak swash plate moment amplitudes as a means of quantifying SBN.

Measurement and simulation results reveal a strong influence of changing line length and the addition of an accumulator on pressure ripple (Δp_{HP}), and swash plate moment amplitudes ΔM_y and ΔM_z; however, sound power was not significantly impacted. The largest SWL reduction overall was 1.8 dBA. Results show a high correlation between SWL and swash plate moment amplitude ΔM_x, which implies that since ΔM_x was not significantly changed, sound power levels were also unchanged. Furthermore, these results indicate that relative contributions of FBN and SBN to-

wards audible noise are highly system and application dependant. For the system studied in this paper, it is likely that devices intended to reduce FBN via silencers would not have a significant impact.

An outcome of this case study is further verification that reduction of noise generation in pumps and motors is only assured if all noise sources are considered. Without the ability to predict and analyze structure borne noise sources, results of sound power radiation would not have been understandable. More importantly, this study also demonstrates the usefulness of predicting transmission noise sources, and how this information is beneficial in the design process of a transmission.

Nomenclature

A	Area	[m^2]
B	Isothermal wave speed	[s/kgm^3]
c	Sound wave speed	[m/s]
D	Diameter	[m]
e	Hose thickness	[m]
E	Young's modulus	[Pa]
f	Darcy-Weisbach coefficient	[m/s]
f_n	Harmonic frequencies	[-]
F	Force	[N]
I	Inertia	[kg m^2]
J	Max line node (at motor)	[-]
K	Bulk modulus	[Pa]
L	Line length	[m]
M	Torque	[Nm]
n	Shaft speed	[rpm]
p	Pressure	[Pa]
P	Power	[W]
Q	Volumetric flow	[m^3/s]
R	Radius	[m]
Re	Reynold's number	[-]
t	Time	[s]
T	Temperature	[°C]
v	Velocity	[m/s]
V	Volume	[m^3]
W	Sound power	[W]
z_K	Number of pistons	[-]
α	Flow coefficient	[-]
β	Swash plate angle	[°]
ρ	Fluid density	[kg/m^3]
φ	Angular position cylinder block	[°]
τ	Shear stress	[Pa]
ν	Kinematic viscosity	[m^2/s]
ω	Angular velocity	[rad/s]

Subscripts

0	First node of HP line
a	Acceleration
b	Block
DC	Displacement Chamber
FM	Fluid Momentum
HP	High Pressure
i	Index of piston
IN	Boundary inlet
j	Index of line
J	Max index of line
k	Piston
LP	Low Pressure
m	Motor
OUT	Boundary outlet
r	Resultant
SB	Block/valve plate
SG	Slipper/swash plate
SK	Piston/cylinder
T	Friction

References

Ashby, B. 2002. Code for computing the numerical solution of a system of first order ordinary differential equations y' = f(x,t). [online] available at HTTP://WWW.unige.ch/~hairer/software.html

Edge, K. A. 1999. Designing quieter hydraulic systems – some recent developments and contributions. *Proceedings Of the Fourth JHPS International Symposium on Fluid Power*, Tokyo, Japan, pp. 3 - 27.

Johansson A. 2005. Design Principles for Noise Reduction in Hydraulic Piston Pumps – Simulation, Optimization and Experimental Verification. PhD thesis, Linkoping University, Sweden.

Klop, R., **Williams, K.**, **Dyminski, D.**, and **Ivantysynova, M.** 2007. A simulation study to reduce noise source of compact power-split-drive transmissions. Proceedings of the 20th Power Transmission and Motion Control Symposium, Bath, England, UK, pp. 83 - 102.

Klop, R. and **Ivantysynova, M.** 2009. A Method of Characteristics Based Coupled Pump/Line Model to Predict Noise Sources of Hydrostatic Transmissions. *Bath ASME Symposium on Fluid Power and Motion Control*, Hollywood, USA, [DSCC2009-2779].

Klop, R. and **Ivantysynova, M.** 2010a. Sound Intensity Measurements to Investigate Noise Generation of Hydrostatic Transmissions. *Proceedings of the 7th International Fluid Power Conference*. Aachen, 2, pp. 229 - 242.

Klop, R. and **Ivantysynova, M.** 2010b. Validation of a Coupled Pump-Motor-Line Model to Predict Noise Sources of Hydrostatic Transmissions. *Proc. of the 6th FPNI PhD Symposium*, Lafayette, IN, USA.

Klop, R. 2010. Investigation of Hydraulic Transmission Noise Sources. PhD thesis, Purdue University, USA.

Kojima, E. and **Ichiyanagi, T.** 2000. Research on Pulsation Attenuation Characteristics of Silencers in Practical Fluid Power Systems. *International Journal of Fluid Power*, 1(2), pp. 29 - 38.

Kojima, E. and **Shinada, M.** 1986. Characteristics of Fluid-borne Noise Generated by a Fluid Power Pump (4th Report, Pressure Ripple in Hydrostatic

Power Transmission). *Bulletin of JSME*, 29 (258), pp. 4147 - 4155.

Nguyen, T. M. and **Elahinia, M.** 2008.Vibration isolation for parallel hydraulic hybrid vehicles. *Shock and Vibration Journal*, 15,pp. 193 - 204.

Schohl, G. A. 1993. Improved approximate method for simulating frequency-dependent friction in transient laminar flow. *Journal of Fluids Engineering*, ASME, 115(3), pp. 420 - 424.

Seeniraj, G. K. 2009. Model based optimization of axial piston machines focusing on noise and efficiency. PhD thesis, Purdue University, USA.

Wieczorek, U. and **Ivantysynova, M.** 2000. Caspar – a computer-aided design tool for axial piston machines. *Proceedings of the Bath Workshop on Power Transmission and Motion Control*, University of Bath, UK, pp. 113 - 126.

Wylie, E. and **Streeter, V.** 1978. *Fluid Transients.* McGraw-Hill Inc. ISBN 0-07-072187-4.

Richard Klop
Born on February 18th 1983 in Kalamazoo Michigan (USA). He received his B.S. Degree from Michigan State University, USA, with high honors in Mechanical Engineering in 2005. He received his Doctorate at Purdue University, USA, in Agricultural and Biological Engineering in 2010. After completing his doctorate, he is working for Parker Hydraulic Systems Division. His main research interests are modeling and design of displacement machines and energy efficient fluid power systems.

Monika Ivantysynova
Born on December 11th 1955 in Polenz (Germany). She received her MSc. Degree in Mechanical Engineering and her PhD. Degree in Fluid Power from the Slovak Technical University of Bratislava, Czechoslovakia. After 7 years in fluid power industry she returned to university. In April 1996 she received a Professorship in fluid power & control at the University of Duisburg (Germany). From 1999 until August 2004 she was Professor of Mechatronic Systems at the Technical University of Hamburg-Harburg. Since August 2004 she is Professor at Purdue University, USA. Her main research areas are energy saving actuator technology and model based optimisation of displacement machines as well as modelling, simulation and testing of fluid power systems. Besides the book "Hydrostatic Pumps and Motors" published in German and English, she has published more than 80 papers in technical journals and at international conferences.